Journal of Materials Chemistry

Cite this: J. Mater. Chem., 2011, 21, 2895

www.rsc.org/materials

PAPER

Color control and white light generation of upconversion luminescence by operating dopant concentrations and pump densities in Yb^{3+}, Er^{3+} and Tm^{3+} tri-doped Lu_2O_3 nanocrystals

Yanping Li,[ab] Jiahua Zhang,*[a] Yongshi Luo,[a] Xia Zhang,[a] Zhendong Hao[a] and Xiaojun Wang[ac]

Received 8th October 2010, Accepted 15th November 2010
DOI: 10.1039/c0jm03394d

We synthesized a series of Yb^{3+}, Er^{3+} and Tm^{3+} tri-doped Lu_2O_3 nanocrystals with various dopant concentrations by the hydrothermal approach. Due to a unique electronic state at the top of the valence band, Lu_2O_3 based materials exhibit intense upconversion luminescence involving $^1G_4 \rightarrow {}^3H_6$ of Tm^{3+} in blue, ($^2H_{11/2}$, $^4S_{3/2}$) $\rightarrow {}^4I_{15/2}$ in green and $^4F_{9/2} \rightarrow {}^4I_{15/2}$ in red of Er^{3+} upon near infrared excitation at 980 nm. The variation of upconversion spectra and color points with dopant concentrations and pump densities are studied in detail on the basis of energy transfer processes. An ideal white upconversion light with color coordinates of (0.327, 0.339) is obtained by controlling the intensity of red, green, and blue emission in $Lu_{1.906}Yb_{0.08}Er_{0.008}Tm_{0.006}O_3$ nanocrystals under a pump density of 8 W cm^{-2}. Based on the present experimental data, we may predict the dopant concentrations and pump densities for any color point within or around the white light region in the tri-doped Lu_2O_3 nanocrystals.

I. Introduction

In recent years, near infrared to visible upconversion luminescence of rare earth ion doped nanomaterials have attracted much attention due to their potential applications in biomedical multicolor imaging, three-dimensional solid-state multicolor displays, and generation of white light sources. To meet the requirements of these applications, upconversion materials are expected to exhibit controllable emission colors, high conversion efficiency, high chemical stability in air, high resistance against laser irradiation damage and so on. In attempts to obtain highly efficient upconversion luminescence, rare earth doped fluorides, such as LaF_3, $NaYF_4$: Er^{3+}, Tm^{3+}, Yb^{3+},[1–3] have been studied extensively for biomedical multicolor imaging due to very low phonon energy (~300 cm^{-1}) in these hosts, which allows for bright upconversion luminescence involving $^1G_4 \rightarrow {}^3H_6$ of Tm^{3+} in blue, ($^2H_{11/2}$, $^4S_{3/2}$) $\rightarrow {}^4I_{15/2}$ in green and $^4F_{9/2} \rightarrow {}^4I_{15/2}$ in red of Er^{3+} upon infrared excitation at 980 nm. However, fluorides are easily hygroscopic in air, limiting their durable use in displays and lighting.

Rare earth oxides, as a promising alternative host matrix for upconversion luminescence, have high chemical stability, low phonon energy (<600 cm^{-1}) and therefore high emission efficiency.[4–7] During the past few years, many studies of white upconversion luminescence in rare earth doped oxides were focused on Yb^{3+}, Er^{3+}, and Tm^{3+} tri-doped Y_2O_3 nanocrystals prepared by different approaches, such as the precipitation method,[8] laser vaporization/controlled condensation (LVCC) technique,[9] and sol–gel process.[10]

Due to a unique electronic state at the top of the valence band and high mass density (9.4 g cm^{-3}), Lu_2O_3 is more challenging *vs.* Y_2O_3 as a host for optical materials. Many investigations have demonstrated that trivalent rare earth ion (Ln^{3+}) doped Lu-based compounds, such as Nd^{3+} doped $LuVO_4$,[11] Ce^{3+}, Pr^{3+} singly doped or Tm^{3+}, Ho^{3+} codoped $LuLiF_4$[12–14] show stronger luminescence and better laser performance than that found for corresponding Y-based compounds. A possible explanation could be found on the basis of an intensity-borrowing mechanism mixing the 4f and 5d orbitals of Ln^{3+} *via* the lattice valence band levels, as proposed by Guillot-Noel *et al.*[15] In fact, in Y-based compounds, the top of the valence band energy levels are mainly composed of oxygen or fluorine 2p orbitals, whereas in Lu-based compounds, the top of the valence bands are composed predominantly of lutetium 4f orbitals. The result is that the valence band-induced mixing of the 4f with the 5d state of Ln^{3+} could be further enhanced in Lu-based compounds, leading to high 4f–4f transition probability of doped rare earth activators and sensitizers. Accordingly, it has been observed that Lu_2O_3 : Er^{3+} shows stronger upconversion luminescence than the Y_2O_3 : Er^{3+} phosphor.[16] Lu_2O_3 is isostructural with Y_2O_3 with a cubic bixbyite crystalline structure. Due to a high mass density, phosphors and/or scintillators with Lu_2O_3 as hosts exhibit

[a]*Key Laboratory of Excited State Processes, Changchun Institute of Optics, Fine Mechanics and Physics, Chinese Academy of Sciences, 3888 Eastern South Lake Road, Changchun, 130033, China. E-mail: zhangjh@ciomp.ac.cn*
[b]*State Key Lab for Mesoscopic Physics and School of Physics, Peking University, Beijing, 100871, China*
[c]*Department of Physics, Georgia Southern University, Statesboro, Georgia, 30460, USA*

a unique advantage of high resistance against laser radiation damage, which is very beneficial to upconverting phosphors. Moreover, the small cell volume also enhances the efficiency of energy transfer between doped ions in Lu_2O_3 in comparison with that in Y_2O_3 for the same fractional doping concentration. Considering the effect of the unique electronic state at the top of the valence band and efficient energy transfer from Yb^{3+} to Er^{3+}, we indeed observed that $Lu_2O_3 : Er^{3+}$, Yb^{3+} shows stronger upconversion luminescence with a larger intensity ratio of red to green emission than $Y_2O_3 : Er^{3+}$, Yb^{3+}, as shown in Fig. 1. As mentioned above, lutetium could be a more favorable cation than yttrium for trivalent rare earth ion doped upconverting phosphors. At present, however, there is only one primary research work by Lin *et al.*[17] on white upconversion luminescence in Yb^{3+}, Er^{3+} and Tm^{3+} tri-doped Lu_2O_3 nanocrystals prepared by a solvothermal process.

In this paper, we demonstrate systematic studies of upconversion luminescent properties as a function of Yb^{3+}, Er^{3+} and Tm^{3+} ion concentrations and pump densities in tri-doped Lu_2O_3 nanocrystals synthesized *via* the hydrothermal approach. The optimal doping concentrations of the tri-dopants and corresponding pump density are obtained for generating ideal white light by controlling the intensity of red, green, and blue emission upon near infrared excitation at 980 nm.

II. Experimental

A. Sample preparation

The typical synthesis of Yb^{3+}, Er^{3+}, and Tm^{3+} tri-doped Lu_2O_3 nanocrystals *via* the hydrothermal approach can be described as follows: the appropriate amounts of Lu_2O_3 (4N), Yb_2O_3 (4N), Er_2O_3 (4N), and Tm_2O_3 (4N) powders were dissolved in dilute nitric acid (G. R.), respectively, to obtain 0.4 M $Lu(NO_3)_3$, 0.02 M $Yb(NO_3)_3$, 0.02 M $Er(NO_3)_3$, and 0.02 M $Tm(NO_3)_3$ solutions. Then, the aforementioned solutions with corresponding mole ratios were mixed and stirred to form a homogeneous solution at room temperature. Subsequently, the pH value of the mixed solution was adjusted to 9 by dropwise addition of dilute ammonium hydrogen carbonate solution (A. R.). After continuous stirring for 1 h, the milky colloidal solution was transferred into a closed Teflon-lined stainless steel autoclave with 50.0 mL capacity, and heated at 200 °C for 3 h. As the autoclave cooled to room temperature, the precipitates were washed with deionized water several times and dried at 65 °C for 14 h in a vacuum oven. The final products were obtained by annealing the precipitates at 950 °C for 1 h in air.

B. Measurements and characterization

The crystalline structure of samples was characterized by X-ray diffraction (XRD) (Rigaku D/max-rA power diffractometer using Cu-Kα ($\lambda = 1.54178$ Å) radiation). Field emission scanning electron microscopy (FE-SEM) images were taken on S-4800 (Hitachi Company) electron microscopes. For upconversion luminescence (UCL) spectra measurement, the powders were pressed to form smooth and flat disks to be utilized for spectral studies by irradiation with a power-controllable 980 nm diode laser, which was coupled to a 200 μm (core) fiber. The focus area on the disk sample was about 2 mm^2. The upconverted visible emissions were collected at right angles with respect to the incident beam by a Triax 550 spectrometer (Jobin-Yvon) and an attached photomultiplier tube.

III. Results and discussion

A. Crystal structure and morphology

Fig. 2 shows the XRD pattern of Yb^{3+}, Er^{3+} and Tm^{3+} tri-doped Lu_2O_3 powder synthesized by the hydrothermal approach. All of the XRD peaks are consistent with the standard X-ray diffraction card JCPDS No. 86-2475 without any impurity peaks, indicating a pure cubic Lu_2O_3 structure. The inset of Fig. 2 is the FE-SEM image of the powder, revealing that the Lu_2O_3 nanocrystals have a nearly spherical shape and an average diameter of about 20 nm.

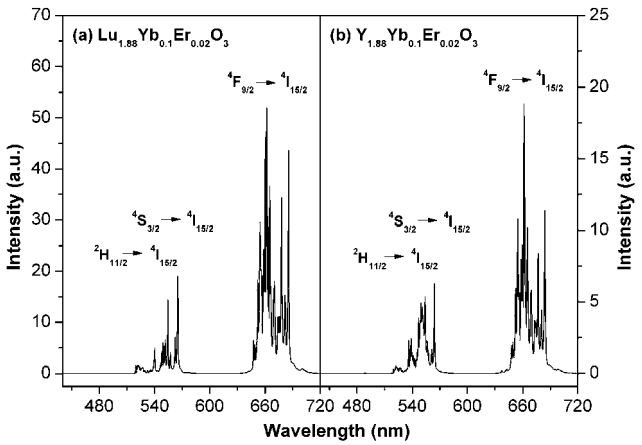

Fig. 1 Comparison of UCL spectra in $Lu_{1.88}Yb_{0.1}Er_{0.02}O_3$ (a) and in $Y_{1.88}Yb_{0.1}Er_{0.02}O_3$ (b) bulk materials under laser excitation at 980 nm, presenting stronger UCL in Lu_2O_3 than in Y_2O_3.

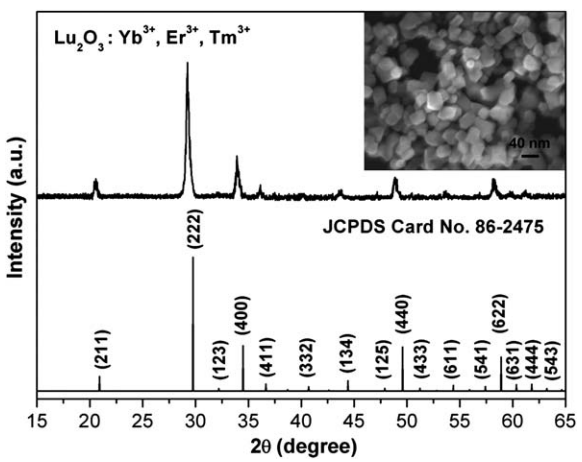

Fig. 2 XRD pattern and FE-SEM image of Yb^{3+}, Er^{3+} and Tm^{3+} tri-doped Lu_2O_3 powder synthesized by the hydrothermal approach.

B. Variation of UCL spectra and color points with dopant concentrations

Fig. 3 displays the UCL spectra of $Lu_{2(1-x)}Ln_{2x}O_3$ nanocrystals (Ln = Yb^{3+}, Er^{3+} or Tm^{3+}) doped with 0.4 mol % Er^{3+} (a), 4 mol % Yb^{3+} and 0.4 mol % Er^{3+} (b), 4 mol % Yb^{3+} and 0.3 mol % Tm^{3+} (c), 4 mol % Yb^{3+}, 0.4 mol % Er^{3+}, and 0.3 mol % Tm^{3+} (d), respectively. The strong blue, green, and red emission lines centered at 485, 550, and 670 nm are well known to originate from the transitions $^1G_4 \rightarrow {}^3H_6$ of Tm^{3+}, $(^2H_{11/2},{}^4S_{3/2}) \rightarrow {}^4I_{15/2}$ of Er^{3+}, and $^4F_{9/2} \rightarrow {}^4I_{15/2}$ of Er^{3+}, respectively. Comparing the spectra in Fig. 3a and 3b, codoping Yb^{3+} in Lu_2O_3 : Er^{3+} strongly enhances the red UCL. The strong blue UCL in Yb^{3+} and Tm^{3+} codoped Lu_2O_3 nanocrystals also reflects the important role of Yb^{3+}, because we cannot detect pronounced UCL in Tm^{3+} single doped Lu_2O_3 nanocrystals. Although a red UCL due to the $^1G_4 \rightarrow {}^3F_4$ transition of Tm^{3+} appears in Lu_2O_3 : Yb^{3+},Tm^{3+} nanocrystals, it is too weak to be considered in this work. Considering the strong effect of dopant concentrations on the color of UCL, we systematically studied the UCL spectra for various dopant concentrations. Finally, we obtained the optimal concentrations of 4 mol % Yb^{3+}, 0.4 mol % Er^{3+}, and 0.3 mol % Tm^{3+} in tri-doped Lu_2O_3 nanocrystals for generating ideal upconverted white light with color coordinates of (0.327, 0.339) under 980 nm pump with power density of 8 W cm^{-2}, as shown in Fig. 3d. The insets in Fig. 3 are the digital images of the corresponding UCL at a pump density of 8 W cm^{-2}.

To control the UCL color, the variation of UCL spectra with each of the Yb^{3+}, Er^{3+} and Tm^{3+} concentrations is studied. Fig. 4a shows the UCL spectra in $Lu_{1.986-2x}Yb_{2x}Er_{0.008}Tm_{0.006}O_3$ nanocrystals with fixed Er^{3+} concentration of 0.4 mol %, Tm^{3+} concentration of 0.3 mol % and variable Yb^{3+} concentrations from 1 mol % to 10 mol %, where the intensities of the red emissions are normalized. Upon increasing Yb^{3+} concentration, the intensity ratios of the green to the red emission decrease rapidly, and finally the green emissions are almost quenched at high concentrations of Yb^{3+}. For better describing the UCL processes, the energy level diagrams of Yb^{3+}, Er^{3+} and Tm^{3+} ions with the indicated pathways of UCL for excitation at 980 nm is illustrated in Fig. 5. The rapid reduction of the green to red ratio can result from two energy transfer processes. One is the transfer from Er^{3+} $^4S_{3/2}$ to Yb^{3+}, depopulating the green emitting state through a cross relaxation: $^4S_{3/2}$ (Er^{3+}) + $^2F_{7/2}$ (Yb^{3+}) $\rightarrow$ $^4I_{13/2}$ (Er^{3+}) + $^2F_{5/2}$ (Yb^{3+}). Another is generally the transfer from Yb^{3+} to Er^{3+}, populating the $^4F_{9/2}$ level described by $^4I_{13/2}$ (Er^{3+}) + $^2F_{5/2}$ (Yb^{3+}) $\rightarrow$ $^4F_{9/2}$ (Er^{3+}) + $^2F_{7/2}$ (Yb^{3+}). It is also clearly observed that the blue emission is enhanced relative to the red with increasing x up to 3 mol %. This is due to the three-photon process of the blue UCL, which is proportional to the third power of the number of Yb^{3+} ions in the excited states, whereas the red UCL is a two-photon process. Where x is higher than 3 mol %, a decrease of the blue emission is observed. A similar phenomenon is also observed in Yb^{3+}, Tm^{3+} co-doped ZrO_2 nanocrystals, and is ascribed to Yb^{3+} induced luminescent quenching.[18] Apparently, the emitting colors of the overall UCL are strongly governed by Yb^{3+} concentrations.

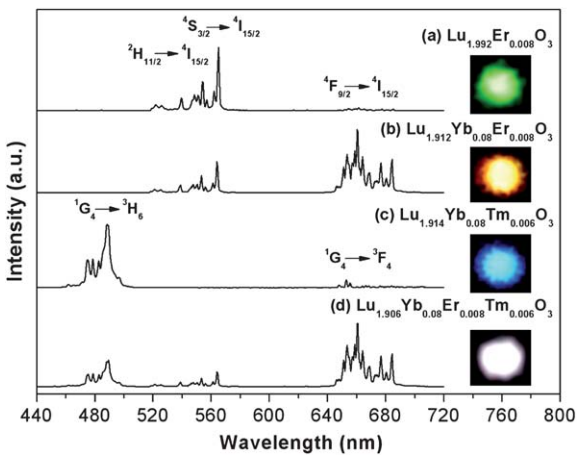

Fig. 3 UCL spectra of $Lu_{1.992}Er_{0.008}O_3$ (a), $Lu_{1.912}Yb_{0.08}Er_{0.008}O_3$ (b), $Lu_{1.914}Yb_{0.08}Tm_{0.006}O_3$ (c), and $Lu_{1.906}Yb_{0.08}Er_{0.008}Tm_{0.006}O_3$ (d) nanocrystals under diode laser excitation at 980 nm with the pump density of 8 W cm^{-2}. The insets are the digital images of the corresponding light emissions.

Fig. 4b displays the UCL spectra of $Lu_{1.914-2x}Yb_{0.08}Er_{2x}Tm_{0.006}O_3$ nanocrystals with fixed Yb^{3+} concentration of 4 mol %, Tm^{3+} concentration of 0.3 mol % and variable Er^{3+} concentrations from 0.1 mol % to 1 mol %, where the intensities of the blue emissions are normalized. One can see the intensities of the green and red emissions of Er^{3+} certainly enhance with increasing Er^{3+} concentration. As a result, the color of the overall UCL changes from greenish blue through white and finally to yellow.

In Yb^{3+}, Er^{3+}, and Tm^{3+} tri-doped Lu_2O_3 nanocrystals, there exists energy transfer between Tm^{3+} ions, leading to quenching of the blue emission for high concentrations of Tm^{3+} through a cross relaxation, as observed in Yb^{3+}, Tm^{3+} codoped Lu_2O_3 and $YLiF_4$.[19,20] We have found the critical concentration of Tm^{3+} is around 0.3 mol % in the tri-doped Lu_2O_3 nanocrystals. To keep a sufficient blue UCL component governed by a three-photon process, we fix the Tm^{3+} concentration to be 0.3 mol % in the two sample series demonstrated in Fig. 4. To determine the effect of Tm^{3+} concentration on UCL color, we have measured the UCL spectra in $Lu_{1.936-2x}Yb_{0.06}Er_{0.004}Tm_{2x}O_3$ nanocrystals with $x = 0$, 0.002, 0.003 and 0.005, as shown in Fig. 6. Besides the reduction of the blue emission due to self-quenching for values of x higher than 0.003, the intensity of the green emission relative to the red reduces monotonously with increasing Tm^{3+} concentration. This behavior can be well explained with a cross energy transfer from the green emitting state of Er^{3+} to Tm^{3+} as described by (1) $^4S_{3/2}$ (Er^{3+}) + $^3H_6$ (Tm^{3+}) $\rightarrow$ $^4I_{9/2}$ (Er^{3+}) + $^3F_4$ (Tm^{3+}) and/or (2) $^4S_{3/2}$ (Er^{3+}) + $^3H_6$ (Tm^{3+}) $\rightarrow$ $^4I_{11/2}$ (Er^{3+}) + $^3H_5$ (Tm^{3+}) (see Fig. 5). Similar transfer processes have been identified in Er^{3+}, Tm^{3+} codoped fluoride crystals.[21] This transfer process is also supported by the observation of lifetime shortening of the green emitting state $^4S_{3/2}$ for high Tm^{3+} concentrations, as shown in Fig. 7.

Based on the spectral data of UCL, the variation of UCL color points as a function of the doping concentrations of Yb^{3+}, Er^{3+} and Tm^{3+} is obtained and illustrated in the Commission Internationale de l'Eclairage France (CIE) 1931 chromaticity diagram, as shown in Fig. 8. For Yb^{3+} concentration as a variable, there appears a crossover at Yb^{3+} concentration of 3 mol %. Below this concentration, the color points shift toward the blue

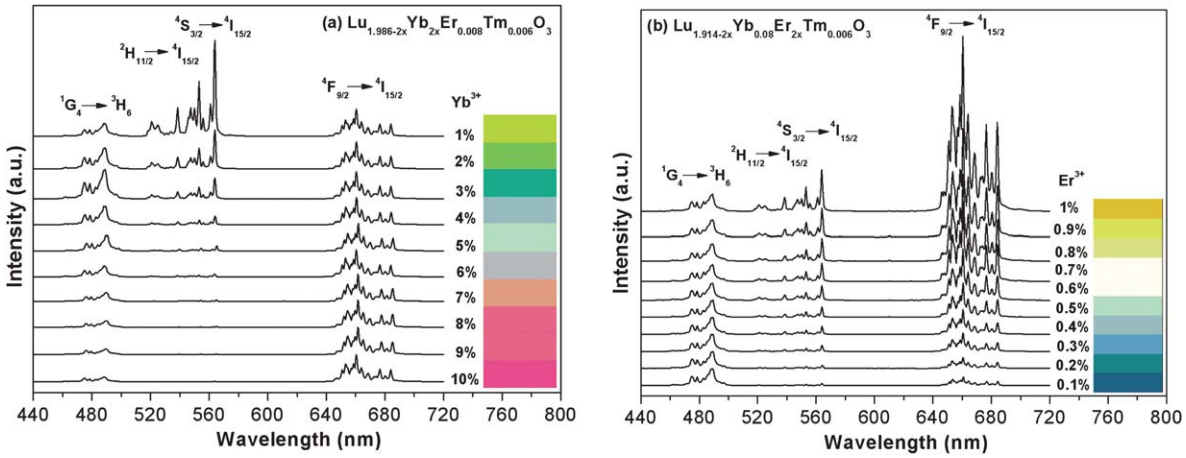

Fig. 4 (a) UCL spectra of $Lu_{1.986-2x}Yb_{2x}Er_{0.008}Tm_{0.006}O_3$ nanocrystals and the corresponding emission colors, the emission intensities are normalized to the red emissions; (b) UCL spectra of $Lu_{1.914-2x}Yb_{0.08}Er_{2x}Tm_{0.006}O_3$ nanocrystals and the corresponding emission colors, the emission intensities are normalized to the blue emissions. The pump density is 15 W cm^{-2} at 980 nm.

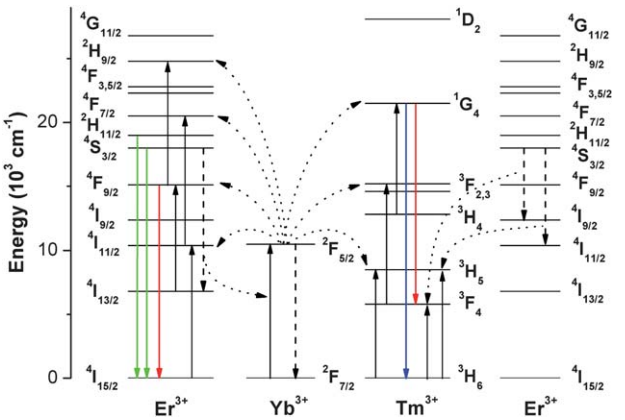

Fig. 5 Energy level diagrams of Yb^{3+}, Er^{3+} and Tm^{3+} ions, as well as the proposed UCL mechanisms under excitation of 980 nm.

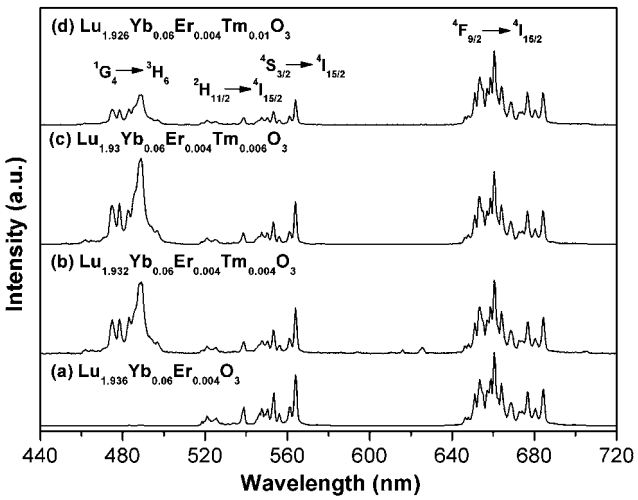

Fig. 6 UCL spectra of $Lu_{1.936}Yb_{0.06}Er_{0.004}O_3$ (a), $Lu_{1.932}Yb_{0.06}Er_{0.004}Tm_{0.004}O_3$ (b), $Lu_{1.93}Yb_{0.06}Er_{0.004}Tm_{0.006}O_3$ (c) and $Lu_{1.926}Yb_{0.06}Er_{0.004}Tm_{0.01}O_3$ (d) nanocrystals under 980 nm laser excitation with the pump density of 15 W cm^{-2}. The emission intensities are normalized to the $^4F_{9/2} \rightarrow {}^4I_{15/2}$ transition.

region due to three photon induced fast enhancement of the blue UCL with increasing Yb^{3+}. Beyond this concentration, the color points turn towards the red region. This is attributed to Yb^{3+} induced quenching of blue and green emissions. The color points fall in the white region for Yb^{3+} concentrations between 4 mol % and 7 mol % in $Lu_{1.986-2x}Yb_{2x}Er_{0.008}Tm_{0.006}O_3$ nanocrystals. For Er^{3+} concentration as a variable, the color points shift directly from blue towards orange with increasing Er^{3+}. This is because increasing Er^{3+} concentration simultaneously raises the green and red UCL without changing their intensity ratio. The color points fall in the white region for Er^{3+} concentrations between 0.3 mol % and 1 mol % in $Lu_{1.914-2x}Yb_{0.08}Er_{2x}Tm_{0.006}O_3$ nanocrystals. In particular, the color points shift gradually from the cold white region to the warm white region with increasing Er^{3+} concentration from 0.3 mol % to 1 mol %. For Tm^{3+} concentration as a variable, there appears to be a retracing point at the quenching concentration of Tm^{3+} at 0.3 mol %. Based on the experimental color points illustrated in Fig. 8, the dopant concentrations for any color point within or around the white light region can be predicted by averaging the adjacent experimental points around the target point of interest.

C. Variation of UCL spectra and color points with pump densities

Due to different numbers of photons involved in the blue UCL and red/green UCL, the spectral distribution varies with the pump density. Fig. 9 shows the UCL spectra for different pump densities of 5 (i), 10 (ii), and 15 (iii) W cm^{-2} in $Lu_{1.906}Yb_{0.08}Er_{0.008}Tm_{0.006}O_3$ nanocrystals, where the emission intensities are normalized to the red. It clearly exhibits that the blue emission increases relative to the red and green as the pump density is increased, leading to a shift of the color point. Fig. 10 shows the pump density dependence of color points in $Lu_{1.906}Yb_{0.08}Er_{0.008}Tm_{0.006}O_3$ nanocrystals under 980 nm excitation. The color points all fall well within the white region, and can be tuned from (0.459, 0.391) to (0.265, 0.323) as the pump density increases from 3 to 15 W cm^{-2}. Particularly, the color coordinate located at (0.327, 0.339), for

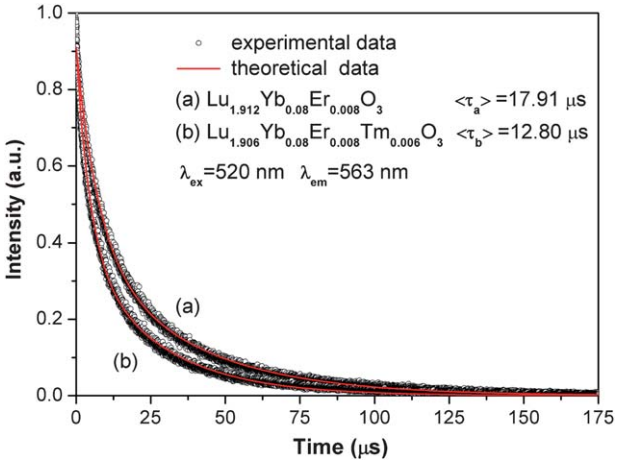

Fig. 7 The fluorescence decay curves of the $^4S_{3/2}$ state of $Lu_{1.912}Yb_{0.08}Er_{0.008}O_3$ (a) and $Lu_{1.906}Yb_{0.08}Er_{0.008}Tm_{0.006}O_3$ (b) nanocrystals.

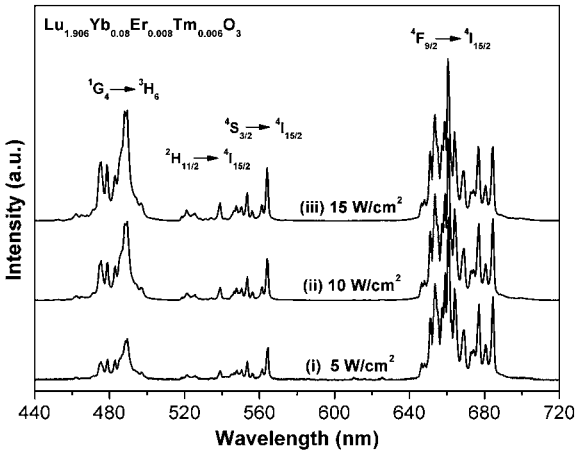

Fig. 9 UCL spectra of $Lu_{1.906}Yb_{0.08}Er_{0.008}Tm_{0.006}O_3$ nanocrystals under diode laser excitation of 980 nm as the pump density increases from 5 (i), to 10 (ii), and finally to 15 (iii) W cm^{-2}. The emission intensities are normalized to the $^4F_{9/2} \rightarrow {}^4I_{15/2}$ transition.

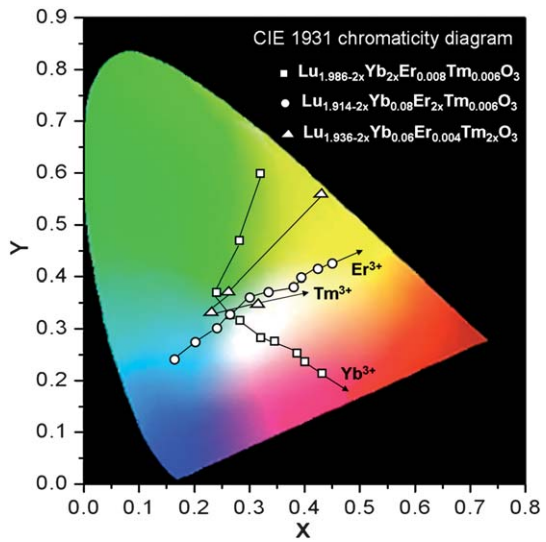

Fig. 8 Variation of UCL color points with increasing Yb^{3+} concentration from 1 mol % to 10 mol % in $Lu_{1.986-2x}Yb_{2x}Er_{0.008}Tm_{0.006}O_3$ nanocrystals, Er^{3+} concentration from 0.1 mol % to 1 mol % in $Lu_{1.914-2x}Yb_{0.08}Er_{2x}Tm_{0.006}O_3$ nanocrystals, and Tm^{3+} concentration from 0, 0.2 mol %, 0.3 mol % to 0.5 mol % in $Lu_{1.936-2x}Yb_{0.06}Er_{0.004}Tm_{2x}O_3$ nanocrystals. The pump density is 15 W cm^{-2} at 980 nm.

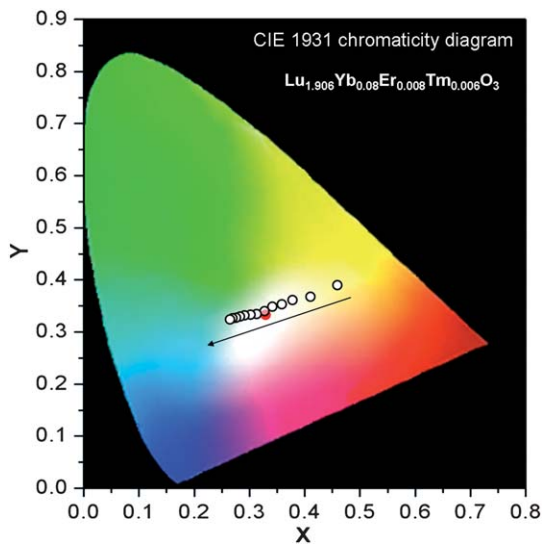

Fig. 10 Variation of UCL color points with increasing pump density from 3 to 15 W cm^{-2} in $Lu_{1.906}Yb_{0.08}Er_{0.008}Tm_{0.006}O_3$ nanocrystals. The red circle is the equal energy white light point (0.33, 0.33).

a pump density of about 8 W cm^{-2}, is very close to the standard equal energy white light illumination (0.33, 0.33). The tendency of the color points towards the blue region upon increasing pump density reflects a faster growth of the blue UCL than the green and red, since the blue UCL is a three-photon process, whereas the green and red UCL are two-photon processes.

To examine the photon number involved in UCL, the dependence of the blue, green and red UCL intensities on pump densities in Yb^{3+}, Tm^{3+} doubly doped, Yb^{3+}, Er^{3+} doubly doped, and Yb^{3+}, Er^{3+}, and Tm^{3+} tri-doped Lu_2O_3 nanocrystals are measured and plotted in logarithmic diagrams as shown in Fig. 11. The photon number n determined from the slope is close to 2 for the red and green UCL and close to 3 for the blue UCL. It should be noted that the n value of 2.56 for the green UCL in the tri-doped system implies notable mixing of a three-photon process, which was proposed to result from transfer from the red emitting state to the green emitting state through the pathway $^4F_{9/2}$ (Er^{3+}) + $^2F_{5/2}$ (Yb^{3+}) → $^2H_{9/2}$ (Er^{3+}) + $^2F_{7/2}$ (Yb^{3+}) (see Fig. 5).[7]

According to the present results of color control by dopant concentrations and pump densities, UCL with various color points can be obtained in Yb^{3+}, Er^{3+}, and Tm^{3+} tri-doped Lu_2O_3 nanocrystals. Using the present data, we may predict the dopant concentrations and pump densities for any color point within or around the white light region in the tri-doped Lu_2O_3 nanocrystals.

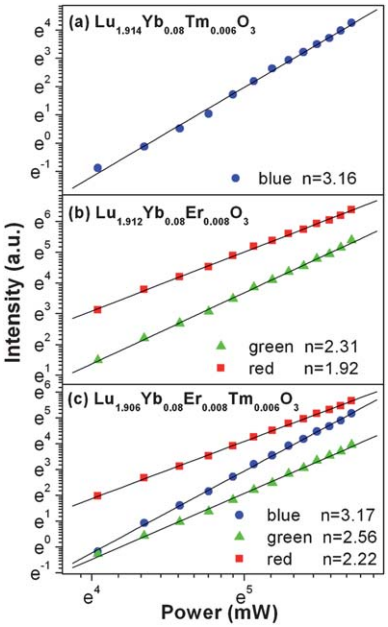

Fig. 11 Power dependence of upconversion emission intensities of $Lu_{1.914}Yb_{0.08}Tm_{0.006}O_3$ (a), $Lu_{1.912}Yb_{0.08}Er_{0.008}O_3$ (b) and $Lu_{1.906}Yb_{0.08}Er_{0.008}Tm_{0.006}O_3$ (c) nanocrystals under 980 nm laser excitation.

IV. Conclusions

In conclusion, we have synthesized Yb^{3+}, Er^{3+} and Tm^{3+} tri-doped Lu_2O_3 nanocrystals with various doping concentrations *via* the hydrothermal approach. The bright upconversion luminescence composed of $^1G_4 \rightarrow {}^3H_6$ emission of Tm^{3+} in blue, $(^2H_{11/2},{}^4S_{3/2}) \rightarrow {}^4I_{15/2}$ of Er^{3+} in green and $^4F_{9/2} \rightarrow {}^4I_{15/2}$ of Er^{3+} in red is obtained under an infrared pump at 980 nm. The color point is strongly governed by dopant concentrations and pump densities. Based on the present experimental data, we may predict the dopant concentrations and pump densities for obtaining any color point within or around the white light region in the tri-doped Lu_2O_3 nanocrystals. An ideal white upconversion light with color coordinates of (0.327, 0.339) is achieved by controlling the intensity of red, green, and blue emission in $Lu_{1.906}Yb_{0.08}Er_{0.008}Tm_{0.006}O_3$ nanocrystals under a pump density of about 8 W cm^{-2}. Due to the unique electronic state at the top of the valence band, high mass density, high chemical stability in air and low phonon energy, Lu_2O_3 based upconverting phosphors could be promising candidates to meet the requirements of high upconverting efficiency and high resistance against laser radiation damage.

Acknowledgements

This work is financially supported by the National Nature Science Foundation of China (10834006, 10774141, 10904141, 10904140), the MOST of China (2006CB601104, 2007CB613402), the Scientific Project of Jilin Province (20090134, 20090524) and CAS Innovation Program.

Notes and references

1 S. Sivakumar, F. C. J. M. Van Veggel and M. Raudsepp, *J. Am. Chem. Soc.*, 2005, **127**, 12464.
2 F. Wang and X. G. Liu, *J. Am. Chem. Soc.*, 2008, **130**, 5642.
3 J. C. Boyer, N. J. J. Johnson and F. C. J. M. Van Veggel, *Chem. Mater.*, 2009, **21**, 2010.
4 D. Matsuura, *Appl. Phys. Lett.*, 2002, **81**, 4526.
5 F. Vetrone, J. C. Boyer, J. A. Capobianco, A. Speghini and M. Bettinelli, *J. Appl. Phys.*, 2004, **96**, 661.
6 Y. Q. Lei, H. W. Song, L. M. Yang, L. X. Yu, Z. X. Liu, G. H. Pan, X. Bai and L. B. Fan, *J. Chem. Phys.*, 2005, **123**, 174710.
7 Y. P. Li, J. H. Zhang, X. Zhang, Y. S. Luo, X. G. Ren, H. F. Zhao, X. J. Wang, L. D. Sun and C. H. Yan, *J. Phys. Chem. C*, 2009, **113**, 4413.
8 G. Y. Chen, Y. Liu, Y. G. Zhang, G. Somesfalean, Z. G. Zhang, Q. Sun and F. P. Wang, *Appl. Phys. Lett.*, 2007, **91**, 133103.
9 G. Glaspell, J. Anderson, J. R. Wilkins and M. Samy El-Shall, *J. Phys. Chem. C*, 2008, **112**, 11527.
10 Y. F. Bai, Y. X. Wang, G. Y. Peng, W. Zhang, Y. K. Wang, K. Yang, X. R. Zhang and Y. L. Song, *Opt. Commun.*, 2009, **282**, 1922.
11 C. Maunier, J. L. Doualan, R. Moncorgé, A. Speghini, M. Bettinelli and E. Cavalli, Advanced Solid-State Lasers, *OSA Trends in Optics and Photonics*, 2001, **50**, 261.
12 C. Maunier, J. L. Doualan, R. Moncorgé and E. Cavalli, *J. Opt. Soc. Am. B*, 2002, **19**, 1794.
13 B. M. Walsh, N. P. Barnes, J. Yu and M. Petros, Advanced Solid-State Lasers, *OSA Trends in Optics and Photonics*, 2002, **68**, 245.
14 V. Sudesh and K. Asai, *J. Opt. Soc. Am. B*, 2003, **20**, 1829.
15 O. Guillot-Noel, B. Bellamy, B. Viana and D. Gourier, *Phys. Rev. B: Condens. Matter*, 1999, **60**, 1668.
16 F. Vetrone, J. C. Boyer, J. A. Capobianco, A. Speghini and M. Bettinelli, *J. Phys. Chem. B*, 2002, **106**, 5622.
17 J. Yang, C. M. Zhang, C. Peng, C. X. Li, L. L. Wang, R. T. Chai and J. Lin, *Chem.–Eur. J.*, 2009, **15**, 4649.
18 A. Patra, S. Saha, M. Alencar, N. Rakov and G. S. Maciel, *Chem. Phys. Lett.*, 2005, **407**, 477.
19 L. Q. An, J. Zhang, M. Liu and S. W. Wang, *J. Alloys Compd.*, 2008, **451**, 538.
20 X. J. Pei, Y. B. Hou, S. L. Zhao, Z. Xu and F. Teng, *Mater. Chem. Phys.*, 2005, **90**, 270.
21 J. P. Jouart, *J. Lumin.*, 1980, **21**, 153.

